Desalination and Water Treatment
www.deswater.com
doi: 10.5004/dwt.2022.28589

264 (2022) 293–306
July

Impact of H_3PO_4-activated carbon from pine fruit shells for paracetamol adsorption from aqueous solution

Imad Hamadneh[a], Rund A. Abu-Zurayk[b], Aseel Aqel[a], Ahmed Al-Mobydeen[c], Lama Hamadneh[d], Yousef Al-Dalahmeh[e], Fayza Hannoon[a], Rula Albuqain[f], Shorouq Alsotari[f], Ammar H. Al-Dujaili[b,*]

[a]*Department of Chemistry, Faculty of Science, University of Jordan, Amman 11942, Jordan, Tel. +962 775500003; email: imad72@hotmail.com (I. Hamadneh), Tel. +962785733913; email: aseelaqel@yahoo.com (A. Aqel), Tel. +962798408852; email: hannonfayza@gmail.com (F. Hannoon)*
[b]*Hamdi Mango Center for Scientific Research, University of Jordan, Amman, P.O. Box: 11942, Jordan, Tel. +962 796 629 774; email: ah.aldujaili@gmail.com (A.H. Al-Dujaili), Tel. +962 799116889; email: r.abuzurayk@ju.edu.jo (R.A. Abu-Zurayk)*
[c]*Department of Chemistry, Faculty of Science, Jerash University, Jerash 26150, Jordan, Tel. +962798962089; email: ahmeddd_mob@yahoo.com (A. Al-Mobydeen)*
[d]*Faculty of Pharmacy, Al-Zaytoonah University of Jordan 11733, Amman, Jordan, Tel. +962777771900; email: lama.hamadneh@zuj.edu.jo (L. Hamadneh)*
[e]*Department of Chemistry, Faculty of Science, Isra University, Amman 11622, Jordan, Tel. +962 795229695; email: yousef.dalahmeh@iu.edu.jo (Y. Al-Dalahmeh)*
[f]*Cell Therapy Center (CTC), The University of Jordan, Amman, 11942, Jordan, Tel. +962798738536; email: buqaien@yahoo.com (R. Albuqain), Tel. +962796605076; email: shalsotari@gmail.com (S. Alsotari)*

Received 16 December 2021; Accepted 19 April 2022

ABSTRACT

The synthesis of activated carbon (AC) from pine fruit shells (PFS) biomass (BM) is described in this paper. AC was made from BM by gradual pyrolysis at 600°C. AC was also chemically activated with H_3PO_4 (BC-H_3PO_4) and pyrolyzed at 600°C. BM, BC, and BC-H_3PO_4 adsorbents were characterized by Fourier-transform infrared spectroscopy, X-ray diffraction, scanning electron microscopy, thermal gravimetric analysis, and elemental analysis. The batch system was used to apply the BM, BC, and BC-H_3PO_4 to the adsorption of paracetamol (PCM) from aqueous solution. Adsorption was evaluated in relation to adsorbent dosage, ionic strength, initial pH solution, contact time, and temperature. Based on their coefficient of determination (R^2), chi-square (χ^2) and error function ($F_{error\%}$) values, equilibrium and kinetic PCM adsorption data revealed that the process obeys the Langmuir, Dubinin–Radushkevich, and pseudo-second-order kinetic equations, respectively. According to the Langmuir model, the highest adsorption capacity for PCM by BM, BC, and BC-H_3PO_4 was 99.010, 166.667, and 256.10 mg/g, respectively. Thermodynamic analysis revealed that PCM adsorption by the adsorbents is spontaneous and exothermic.

Keywords: Activated carbon; Chemical activation; Phosphoric acid; Adsorption

* Corresponding author.

1. Introduction

In recent years, more pharmaceuticals have been found in sewage wastewater, surface water, and groundwater due to the widespread use of various drugs. Many of these pharmaceutical compounds are commonly used as an anti-inflammatory, analgesic, antibiotic, preservative, and disinfectant [1].

Paracetamol (PCM), named as 4-acetamidephenol, 4-hydroxyacetanilide or acetaminophen, is commonly used as an antipyretic and analgesic for human consumption and veterinary usage for the treatment of headaches, fever and other minor pain worldwide [2–4]. PCM discharges into the aqueous environment from different waste water types, such as municipal wastewater and pharmaceutical processing facilities. As a consequence, it has been listed as one of the most common organic contaminants found in various bodies of water [5].

PCM is toxic to organisms living in water and land, even at very low concentrations. In addition, it has been found to have an endocrine-disrupting effect on some fish and crustacean species. This contributes in some cases to disturbance in the production of offspring, developmental defects, changes in sex hormones, and increasing mortality. In domestic sewage [6] and hospital wastewater [7], PCM concentrations reach 338 ng/L and 150 g/L, respectively. The greatest concentration of PCM recorded in surface water in African countries, many of which lack wastewater treatment plants, was 215 times greater than that reported in European surface waters, according to a recent study [8]. To limit the occurrence of pharmaceutical toxins in these settings, it is essential to develop effective treatment processes to limit the presence of pharmaceutical pollutants in these environments.

Ozonation [9], hydrogen peroxide-based oxidation [10], sonolysis [11], photo-Fenton method [12], photocatalysis [13], and electrochemical oxidation on stainless steel have all been tested for PCM treatment due to its stability under conventional treatment processes [14]. Recently removal of aqueous PCM by biodegradation electrochemical, and photocatalysis has been reported for degradation of PCM [15].

Activated carbon is a solid carbon material with an amorphous structure produced from agricultural biomass (wood, peat, bones, cellulose, and any other agricultural wastes) through a pyrolysis process. The main advantage of using activated carbon to remove pharmaceuticals is that it does not generate toxic or pharmacologically active products. According to the literature, extremely high surface area, porosity, and other surface properties make activated carbons a versatile and universally acclaimed adsorbent [16].

Activated carbon has many applications in industry and medical fields such as refining processes, gas masks, wastewater treatment [17], air cleaning, silage agent [18] and an antidote for many types of drug poisoning [19].

The ability of wastes (mainly agricultural residues) has actually been demonstrated as precursors of low-cost activated carbons and the effective use of these materials for the removal of aqueous solution contaminants [20–23]. Activated carbons are made from materials rich in carbon through carbonization and an activation process. A porous structure and its adsorption properties can be obtained in carbonaceous materials via either physical or chemical activation. Physical activation involves pyrolysis of the source material at 600°C–800°C to produce charcoal. This is then followed by activation using steam, carbon dioxide (CO_2) or oxygen (O_2). Chemical activation involves the impregnation by a chemical activating agent such as phosphoric acid (H_3PO_4) of the precursor material, accompanied by activation at a certain temperature under a minimal atmosphere of oxygen or nitrogen. H_3PO_4 is commonly used as an activating chemical agent. Activating chemical agents affect the decomposition of pyrolytes and prevent tar and volatile matter formation, thus increasing the activated carbon yield [24,25].

Several studies have been carried out on the preparation of activated carbon from waste from pine trees. For example, for the removal of inorganic or organic pollutants such as nickel, copper, and lead, pine cone shell, pine cone powder, pine fruit shell was used [26,27], textile dyes, phenol [28–31], and pine cone activated carbon to remove lead, hexavalalent, phenol and methylene blue [32,33] from aqueous solutions. Since this waste is available in large amounts in the Mediterranean region and is of no commercial value, the shell of the pine cone may be a promising low-cost biomaterial adsorbent.

The effect of the pyrolysis temperature on the preparation of activated carbon from pine fruit shells has been recently reported by us [34]. The optimum temperature of 600°C was selected in light of the results of this analysis. In this work, this sample was chemically activated with H_3PO_4 to study the influence of chemical activation.

The main objective of this study is therefore to prepare pine fruit shell activated carbon by chemical activation using H_3PO_4 followed by pyrolysis at 600°C in order to obtain abundant low-cost activated carbon, green and environmentally healthy agricultural by-products. They were used for the removal of PCM from aqueous solution as adsorbents. To understand the adsorption process, the kinetic data and equilibrium data on batch adsorption studies were carried out. There are also study of the effects of adsorption parameters such as dosage effect, initial pH, contact time and temperature.

2. Materials and methods

2.1. Materials and instruments

Pine fruit shells (PFS) collected from The University of Jordan trees in Amman. PCM drug in powder form taken from Dar Al Dawa Company in Jordan (purity > 99.9). H_3PO_4, NaOH, HCl and NaCl were obtained from Sigma Aldrich Chemicals Company (Saint Louis, MO, USA 63178) with purity higher than 99% and used without further purification. A Protherm-PC 402 tube furnace model (Turkey) was used to prepare activated carbon. The Precisa 410AM-FR analytical balance (CH-8953 Dietikon, Switzerland) was used to weigh the samples. Elemental analysis was carried out using an elemental analyzer (Euro Vector) to determine the elemental composition (C, H and N) before and after pyrolysis and activation. Fourier-transform infrared spectroscopy (FTIR) analysis was performed in the solid state to determine the surface functional groups. This was obtained

using an infrared spectrometer: Thermo Nicolet NEXUS 670 Fourier transform infrared spectrometer (Waltham, MA USA 02451). Using a PANalytical X'Pert PRO X-ray diffractometer (Eindhoven, Netherlands), X-ray diffractograms were acquired to identify the extent of crystallinity or amorphous nature of the samples. The experiment was carried out with a Cu-Kα radiation source and a diffraction angle (2θ) range of 4°–60°. Morphological studies were obtained using a scanning electron microscope (SEM): FEI inspects F50 (Tulsa, OK 74145), accelerating voltage and beam current 30 kV. The thermal gravimetric analysis (TGA) of the dried samples was studied using NETZSCH STA 409 PG/PC Thermal Analyzer (Leipzig, Germany) in the temperature range (25°C–600°C), at a heating rate of 10°C/min. The GFL 1083 shaker was used to collect the samples. The thermostat-equipped GFL 1083 shaker was used for the shaking. PCM concentration was measured using a UV-Vis Cary Varian spectrophotometer (UK).

The samples' pore structure and activated carbon surface area were determined using a Nova 2200 e sSurface area and pore size Analyzer (Quantachrome Corp., Boynton Beach, FL, USA) after nitrogen gas adsorption/desorption isotherms were measured at 77 K. At 105°C, each sample was degassed for 8 h. The Brunauer, Emmett, and Teller (BET) equation was used to get the specific surface area, and total pore volume (V_{total}) was derived using the near saturation uptake (P/Po = 0.99). The average pore diameters (D_{ap}) were estimated from the SA_{BET} and V_{total} assuming an open-ended cylindrical pore model without pore networks [35].

2.2. Preparation of BC and BC-H_3PO_4

PFS was manually separated from the fruit seeds, and extensively washed with water to get rid of any dirt or impurities from the surface, dried at 105°C for 24 h and then grounded to ≤1 mm size. Three samples were taken from the dried PFS. The first one is a biomass (BM) was used without any further modifications. The second sample was placed in covered crucibles and heated in a tube furnace at 600°C under oxygen-limited conditions for duration of 3 h and labeled as BC. The third part was chemically activated with H_3PO_4. Chemical activation was accomplished by soaking for 24 h in 30% ortho-phosphoric acid (H_3PO_4) with impregnation ratios of 1BM:4H_3PO_4 (w/w). The sample was then filtered with a vacuum pump and dehydrated in a 105°C oven overnight. The dried sample was then pyrolyzed for 3 h at 600°C in order to activate it. The material was allowed to cool to room temperature after the activation. The activated carbon was then labeled as BC-H_3PO_4 and washed with 1.0 M NaOH before being rinsed with hot distilled water and then cold distilled water until the filtrate achieved a pH of 6–7. The sample was then dried for 24 h at 105°C in an oven. The three samples were further crushed and sieved to get the particles size of 200–300 μm and stored in air tight desiccators for further uses.

2.3. The pH at point zero charge (pH_{PZC})

The pH of the BM, BC and BC-H_3PO_4 adsorbents at point zero charge (pH_{PZC}) was calculated by solid addition [36] by moving 50 mL KNO_3 to a series of 100 mL conical flasks. The initial pH (pH_i) of this solution was modified roughly from 2 to 10 with either 0.1 M HCl or 0.1 M NaOH solutions. pH_i of the solution was correctly observed and 0.1 g of BM, BC and BC-H_3PO_4 was applied to each flask. The flasks were allowed to be balanced for 24 h with occasional manual shaking. The final pH values of the supernatant liquid were observed (pH_f). The differentiation of pH_i and pH_f values was plotted against pH_i. As pH_{PZC}, the intersection point of the resulting curve noted the difference between pH = 0.0.

2.4. Moisture and ash content

The yield of activated carbon was calculated based on the weight of BM on a dry basis from the following equation:

$$\text{Yield}\% = \frac{\text{weight of activated carbon}}{\text{weight of biomass}} \times 100 \quad (1)$$

Moisture and ash content were calculated according to ASTM D1762-84 standards by measuring weigh loss difference for samples dried at 105°C for 24 h after being cooled in desiccators for about 15 min using the following equations [37,38]:

$$\text{Moisture content}\% = \frac{\text{wet weight} - \text{dry weight}}{\text{dry weight}} \times 100 \quad (2)$$

$$\text{Ash content}\% = \frac{\text{mass of ash}(\text{g})}{\text{dry mass of sample}(\text{g})} \times 100 \quad (3)$$

2.5. Adsorption experiment and procedures

2.5.1. Batch experiment

A batch adsorption experiment was conducted with a solution containing 50 mg/L of PCM as the beginning concentration. In 250 mL Erlenmeyer flasks containing 0.10 g BM, BC or BC-H_3PO_4, the experiment was carried out. The flask was shaken for 24 h in an electric shaker, and then the contents were centrifuged at 3,000 rpm for 6 min to ensure that the PCM solution and the adsorbent were separated, and the flask was filtered using 0.22 μm filters. Concentration of PCM was calculated using UV-visible spectrophotometer at 242.48 nm. The amounts of PCM (q_e mg/g) and the percentage removal of adsorption (%R) adsorbed by the BM, BC and BC-H_3PO_4 were calculated using the following equations:

$$q_e = \frac{(C_o - C_e)V}{m} \quad (4)$$

$$\%R = \frac{(C_o - C_e)}{C_o} \times 100 \quad (5)$$

where q_e (mg/g) is the amount of PCM adsorbed by the BM, BC and BC-H_3PO_4, C_o and C_e (mg/L) are the initial and equilibrium concentration of PCM, respectively, V (L) the

initial volume of PCM solution and m (g) the weight of the adsorbent.

2.5.2. Effect of adsorbent dosage

Different solutions from BM, BC and BC-H_3PO_4 with different weights of 0.01, 0.02, 0.03, 0.04, 0.05, 0.075, 0.100, 0.15, 0.20 g were mixed separately with 50 mL of 50 mg/L PCM solution, placed in a water bath shaker at 25°C and kept overnight, the supernatants were filtered using 0.22 μm filters.

2.5.3. Effect of pH

Adsorption of paracetamol via BM, BC and BC-H_3PO_4 surfaces was measured at concentrations of 50 mg/L PCM. pH value for the solutions was adjusted from 2–10 using HCl (0.1 M) and NaOH (0.1 M) solutions.

2.5.4. Effect of ionic strength

NaCl solutions with different concentrations of 0.01, 0.05, 0.10, 0.15 and 0.20 M were added separately to solutions containing 0.50 g of adsorbent and 50 mg PCM/L NaCl proper concentration solution at 25°C, the above-mentioned protocol of filtration was applied.

2.5.5. Adsorption isotherm

Ten PCM solutions with different concentrations of 10, 20, 30, 40, 50, 60, 70, 80, 90 and 100 mg/L were prepared from PCM stock solution (1,000 mg/L) and added separately to 0.15 g of adsorbent in a stopper Erlenmeyer flask. The solutions were placed in a water bath shaker at different temperatures of 25°C, 35°C, 45°C for 24 h. Solutions were allowed to settle down, centrifuged and filtered using micro filters. Adsorption was measured at the corresponded λ_{max} (242.48 nm) and C_e value was obtained from the calibration curves.

The results were fitted to Langmuir, Freundlich and Dubinin–Radushkevich (D-R) isotherm models [39–41]:

Langmuir equation:

$$q_e = \frac{q_{\max} K_L C_e}{1 + K_L C_e} \tag{6}$$

where q_e is the quantity of PCM absorbed by the adsorbents (mg/g), q_{max} is the monolayer capacity of the adsorbent (mg/g), K_L is the Langmuir binding constant (L/mg). The dimensionless separation factor (R_L) of Langmuir is used to predict the affinity between the PCM solution and the adsorbents. R_L can be calculated by the following equation:

$$R_L = \frac{1}{1 + C_o K_L} \tag{7}$$

where C_o is the highest initial PCM concentration in the solution (mg/L). This is often used to judge whether adsorption process is a thermodynamically favorable process or not: $R_L > 1$ it is an unfavorable adsorption; $R_L = 1$, indicates a linear adsorption; when $0 < R_L < 1$, adsorption is favorable; when $R_L = 0$, it is an irreversible adsorption [42].

Freundlich equation:

$$q_e = K_F C_e^{1/n} \tag{8}$$

where K_F is the Freundlich constant [mg/g(L/mg)$^{1/n}$] indicating the adsorption capacity, n is the empirical constant indicating the adsorption intensity,

D-R equation:

$$q_e = q_{\max} \exp\left(-K_{\mathrm{DR}} \left[RT \ln\left(1 + \frac{1}{C_e} \right) \right]^2 \right) = q_{\max} \exp\left(-K_{\mathrm{DR}} \varepsilon^2 \right) \tag{9}$$

where ε is the polanyi potential equivalent to RT ln(1 + 1/C_e), K_{DR} is the mean free adsorption energy per adsorbate molecule, R, and T are the gas constant (8.314 J/mol K) and temperature (K), respectively. E_{DR} (kJ/mol) is the mean free adsorption energy per adsorbent molecule when transported from infinity to the solid surface in the solution, which provides chemical or physical adsorption data, which may be calculated using the equation:

$$E_{\mathrm{DR}} = \left(2K_{\mathrm{DR}} \right)^{-1/2} \tag{10}$$

2.5.6. Kinetic studies

The study of adsorption kinetic was achieved by preparing a PCM solution of 50 mg/L followed by mixing with 0.15 g of adsorbent over a time period of 0, 5, 10, 20, 30, 40, 60, 90, 120, 150, and 180 min, these solutions were placed in a water bath at 25°C.

The kinetics of the adsorption were modeled using the pseudo-first-order rate of Lagergren, pseudo-second-order and Weber–Morris intraparticle diffusion kinetic models [43–45]:

Pseudo-first-order:

$$q_t = q_e \left(1 - e^{-k_1 t} \right) \tag{11}$$

Pseudo-second-order:

$$q_t = \frac{k_2 q_e^2 t}{1 + k_2 q_e t} \tag{12}$$

Intraparticle diffusion:

$$q_t = k_{\mathrm{int}} t^{0.5} + C \tag{13}$$

where q_t (mg/g) is the quantity of PCM adsorbed at any time, k_1 is the pseudo-first-order constant (min^{-1}), k_2 is the pseudo-second-order constant (g/mg min) and k_{int} is the intraparticle diffusion rate constant (mg/g min$^{1/2}$) and C is a value of intercept constant.

2.6. Statistical evaluation

The linear correlation coefficient (R^2) was used to express the conformity between the experimental data and the model expected values. The best fit to the equilibrium and kinetic models was determined by a relatively high R^2 value (close or equal to 1). The R^2 was calculated according to Eq. (14) [46].

$$R^2 = \frac{\sum\left(q_{e,\text{cal}} - q_{e,\text{mean}}\right)^2}{\sum\left(q_{e,\text{cal}} - q_{e,\text{mean}}\right)^2 + \sum\left(q_{e,\text{cal}} - q_{e,\text{exp}}\right)^2} \tag{14}$$

Furthermore, the applicability of each model for the respective adsorption scheme is investigated by measuring the chi-square (χ^2) and the error function ($F_{\text{error\%}}$) [47], as shown by Eqs. (15) and (16):

$$\chi^2 = \sum \frac{\left(q_{e,\text{exp}} - q_{e,\text{cal}}\right)^2}{q_{e,\text{cal}}} \tag{15}$$

$$F_{\text{error\%}} = 100 \times \sqrt{\sum_{i}^{N}\left[\frac{q_{e,\text{exp}} - q_{e,\text{cal}}}{q_{e,\text{exp}}}\right]^2 / \left(N - P\right)} \tag{16}$$

In the present study we have also applied Akaike's information criterion (AIC) [48] to know the efficacy of the models without seeing the effect of number of parameters in the model. Accordingly, the model with least AIC value would be the best model. In order to evaluate AIC, we need to know error sum of squires (SSE). It is calculated based on the sum of squires of difference between experimental and calculated values. It can be expressed as

$$\text{SSE} = \sum\left(q_{e,\text{exp}} - q_{e,\text{cal}}\right)^2 \tag{17}$$

Mathematically AIC is expressed as

$$\text{AIC} = N \ln\left(\frac{\text{SSE}}{N}\right) + 2P \tag{18}$$

If the numbers of data set points are less 40 then we have to use $\text{AIC}_{\text{corrected}}$. It is defined as follows.

$$\text{AIC}_{\text{corrected}} = \text{AIC} + \frac{2P\left(P+1\right)}{N - P - 1} \tag{19}$$

where $q_{e,\text{exp}}$ (mg/g) is the equilibrium quantity of PCM extracted from Eq. (4), $q_{e,\text{cal}}$ (mg/g) is the quantity of PCM extracted from the models and $q_{e,\text{mean}}$ (mg/g) is the mean of $q_{e,\text{exp}}$ values, N is the number of experimental information points, P is the number of model parameters.

2.7. Thermodynamic studies

Thermodynamic properties were assessed by mixing 50 mg/L of PCM solution with 0.15 g of adsorbent at different temperatures of 25°C, 35°C, and 45°C for 24 h.

3. Results and discussion

3.1. Characterization of adsorbents

The BM, BC and BC-H_3PO_4 were characterized using X-ray diffraction (XRD), SEM, TGA, FTIR, elemental analysis (C, H, and N), pH_{pzc} measurements, moisture content% and ash content%.

3.1.1. Yield and physico-chemical properties of adsorbents

Table 1 summarizes the yield percentage, textural properties and physico-chemical properties of BM, BC and BC-H_3PO_4, including ash content percentage, moisture percentage and elemental study. The results showed that pyrolysis and H_3PO_4 activation had a major effect on the properties of BC and BC-H_3PO_4. The BC yield was much higher than the BC-H_3PO_4 yield. This can be due to the implementation of the content of the triggering agent H_3PO_4 [24]. BC and BC-H_3PO_4 possess greater carbon content relative to the original BM. In addition, BC's ash content is greater than both BM and BC-H_3PO_4, which is consistent with the literature [49]. This can be explained by the increase in the percentage of inorganic matter in BM and BC-H_3PO_4.

According to the activated carbon textural properties, as expected, the prepared activated carbon exhibited a high porosity and total pore volumes. The SA_{BET} (1,022.13 m^2/g) and V_{total} (0.566 cm^3/g) values of BC-H_3PO_4 are higher than this SA_{BET} (237.71 m^2/g) and V_{total} (0.122 cm^3/g) of BC (Table 1). These results could be due to increasing micropore and mesopore volume. Similar results were reported by Nourmoradi et al. [50] and Wong et al. [51] they prepared activated carbon from *Quercus brantii* (oak) acorn and spent tea leaves for the adsorption of PCM, respectively. The generated activated carbons with a large specific surface area and well-developed internal pore structure

Table 1
Basic physico-chemical characteristics of the BM, BC and BC-H_3PO_4

Analysis	BM	BC	BC-H_3PO_4
Yield%		29.23	17.68
Ash%	3.67	14.03	7.17
Moisture%	0.07	0.06	1.71
Acid extractable content%	0.027	0.063	0.057
pH_{zpc}	6.07	6.71	7.13
SA_{BET} (m^2/g)		237.71	1022.13
V_{total} (cm^3/g)		0.122	0.566
r_{BET} (nm)		1.605	1.108
D_{ap} (nm)[a]		2.053	2.215
C%	49.46	81.12	25.68
H%	6.88	2.53	4.73
N%	0.26	0.60	0.00
O%	43.40	15.75	69.59
H/C	0.139	0.031	0.148
(O+N)/C	0.883	0.202	2.710

[a]calculated as = 4 V_{total}/SA_{BET}.

are expected to properly adsorb the PCM molecules in solution via a pore-filling mechanism.

The elemental analysis showed that BC's carbon content increased from 49.46% (BM) and 25.68% (BC-H_3PO_4) to 81.12%. The polarity index (O+N)/C ratios increased to 2.71% for BC-H_3PO_4 is an indication of the surface polar functional groups induced by activation with H_3PO_4. On the other hand, the decrease in the H/C ratio provided an indication of the degree of carbonization and aromaticity, indicating that the BC progressively became more carbonaceous and aromatic with pyrolysis and activation as a result of the progressive dehydration and decarboxylation reaction [52,53]. The BM, BC and BC-H_3PO_4 had shown various acid extractable content%. It can be seen that pyrolysis and activation conditions had significant influence on the presence of basic cations in the adsorbents. During adsorption, these cations in the BC and BC-H_3PO_4 ash can be released and more vacant sites are developed and hence, the adsorption capacity is increased [9].

3.1.2. FTIR spectra

This technique is useful in confirming the existence of certain functional groups in an adsorbent originally present, pyrolysis or added by chemical activation [54]. For comparison, Fig. 1 shows the FTIR spectrum of BM, BC and BC-H_3PO_4 which have the following absorption bands:

The bands seen at 3,507–3,586 cm^{-1} indicate the presence of alcohol, phenol, and carbonyl groups, as well as the OH stretching vibration. The bands at 1,600 cm^{-1} are caused by aromatic C=C and C=O stretching modes in conjugated ketones and quinones, whereas the band at 1,422 cm^{-1} is caused by aromatic C–C stretching vibrations in the aromatic ring. Because H_3PO_4 can be effectively removed by washing with water, the entire bands at 1,156; 1,146 and 1,139 cm^{-1} for BC-H_3PO_4 indicate $u_{C–O}$ stretching vibrations in alcohols, phenols, and ether groups and can also be assigned to vibrations of hydrogen bonds P–O to C–O to that of vibrations of bonds P–O–C (aromatic) and P–OOH or P–O–P resulted from the interaction of the H_3PO_4 with the molecule of the BC [55]. The weak bands for BC-H_3PO_4 at 1,058; 1,037 and 1,072 cm^{-1} may be related to chemical bonding of ionized P^+–O– in acid phosphate esters and symmetric vibrations in strings of P–O–P (polyphosphate) [56] or to the presence of R–OH groups [57].

3.1.3. X-ray diffraction analysis

The crystalline structure of the BM, BC and BC-H_3PO_4 is presented by XRD patterns in Fig. 2. XRD pattern for BM shows a typical feature for crystalline cellulose (monoclinic structure) as characterized by the existing three peaks at 2θ = 16.5° with (110), 2θ = 22.5° (200) and 2θ = 34.6° (004) these results are in good match with [58]. However, unknown peaks were also existed at 2θ = 37.78° and 2θ = 43.94°. After thermal treatment at 550°C, dramatic changes occurred in the BC sample, with the above-mentioned peaks disappearing and being replaced by an amorphous structure. Furthermore, thermal treatment raised the peak intensities for 37.78° and 43.9°, since increasing temperature causes small holes to collide with one another, resulting in larger pores. This finding is consistent with previous research [59]. After acid activation (BC-H_3PO_4), all the peaks were disappeared and an amorphous structure, with a broad peak formation at 2θ ranged from 8.0°–30.0° was observed. This change is expected due to the etching process to the internal and external surfaces that lead to irregular and distorted structure for BC-H_3PO_4.

3.1.4. Scanning electron microscopy

In Fig. 3a the SEM micrograph of BM shows a smooth surface with a layered-like structure and very few gaps and pores observed. More folds and pores (observed in the layered structure of BC are shown in the surface structure (Fig. 3b). After acid activation, which is supposed to increase the inner surface area, Fig. 3c shows a large number of pores, which indicates that the porous nature of BC-H_3PO_4 is a desired feature for adsorption.

3.1.5. Thermal gravimetric analysis

Fig. 4 shows the SEM images of the BM, BC and BC-H_3PO_4. The TGA thermogram for BM indicates three big drops with the entire weight loss is more than 70% as a function of temperature, the first drop lies at temperatures between 40°C–100°C which is due to the adsorbed water, the second one lies between 100°C–200°C which is due to the

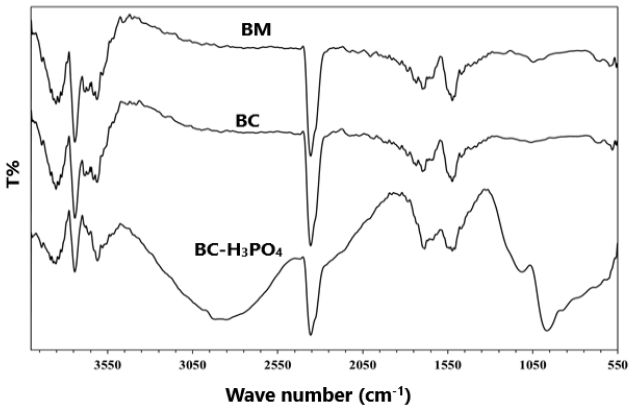

Fig. 1. FTIR spectra of BM, BC and BC-H_3PO_4.

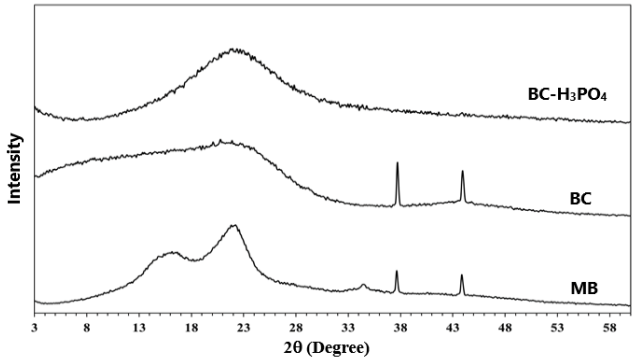

Fig. 2. XRD pattern of BM, BC and BC-H_3PO_4.

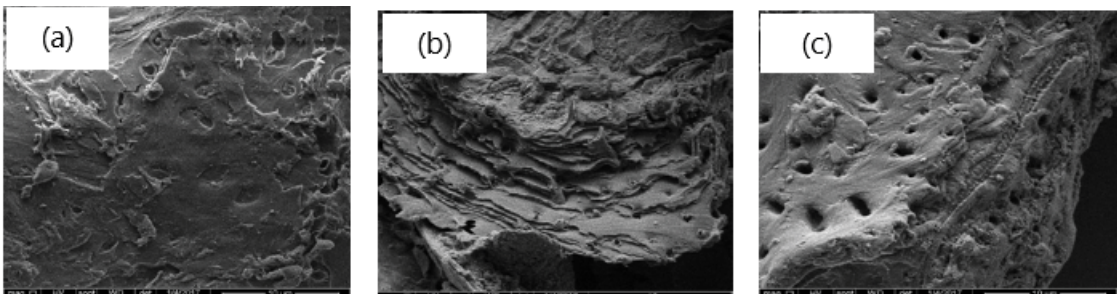

Fig. 3. SEM micrograph for (a) BM, (b) BC and (c) BC-H_3PO_4.

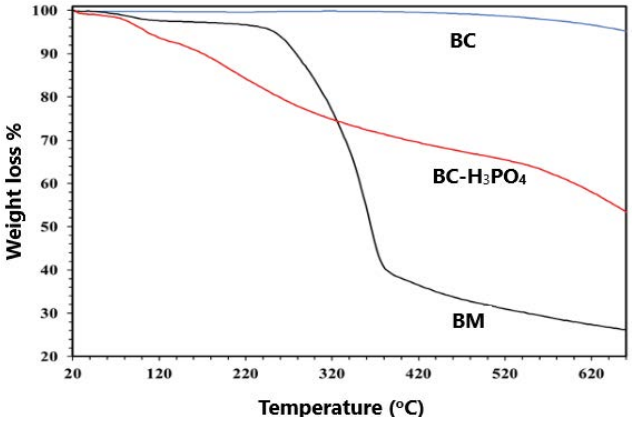

Fig. 4. TGA thermogram for BM, BC and BC-H_3PO_4.

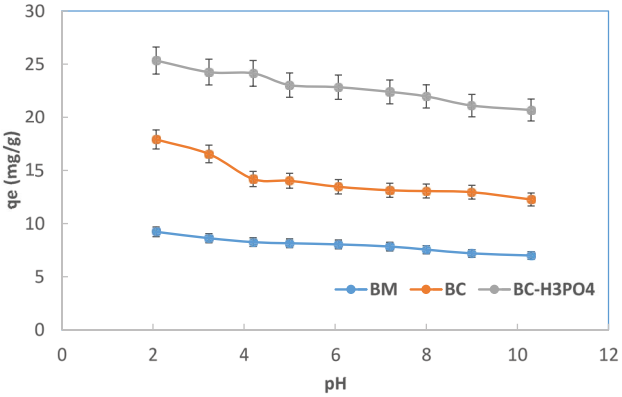

Fig. 5. Effect of pH on the adsorption of PCM onto BM, BC and BC-H_3PO_4. Initial PCM concentration 50 mg/L; adsorbent dosage 0.15 g/50 mL; temperature 25°C.

loss of crystallinity (trapped within the cellulose fibers), and the third drop lies between 220°C–400°C which is due to the decomposition of cellulose into carbon dioxide and water. The thermogram of BC clearly shows a stable thermogram, and a small change in weight loss (5%). However, the weight loss (45%) was observed when a BC sample was chemically activated with H_3PO_4 and expected to have high porosity materials.

3.2. Effect of adsorbent dosage

Different experiments ranging from 0.01–0.20 g/50 mL adsorbent dosages given in Fig. S1 were performed to optimize the dosage of BM, BC, and BC-H_3PO_4. Paracetamol percentage removal has been shown to increase as the quantity of BM, BC, and BC-H_3PO_4 rises to 0.15 g/50 mL. It can be understood that with the increased amount of adsorbents, the percentage removal increases due to the increasing amount of binding sites of the BM, BC, and BC-H_3PO_4 for the PCM molecule [60]. Increasing further the dosage was found to have no significant effect on the % removal of the PCM. The optimum quantity of BM, BC and BC-H_3PO_4 for PCM removal was calculated to be 0.15 g/50 mL based on these findings, and this quantity was used in subsequent experiments.

3.3. Effect of solution pH and ionic strength

In general, two essential parameters influence the adsorption mechanism of an adsorbent: solution pH and ionic strength. This is due to the fact that these two parameters have a significant impact on the properties of the adsorbent's charge surface and the species of adsorbate. Within the pH range of 2.1–11.3 and ionic strength of 0.01–0.20 M NaCl, the effects of initial pH and ionic strength on the amount of PCM adsorption using BM, BC, and BC-H_3PO_4 adsorbents were investigated (Figs. 5 and S2). Over the pH and ionic strength range a slight change in PCM adsorption was observed. Since BM, BC, and BC-H_3PO_4 have an amphoteric aspect, its charge surface is often changing in response to the pH solution and its pH point zero charge (pH_{PZC}). The pKa values of PCM obtained by the Raman spectroscopic technique and the potentiometric process, according to Elbagerma et al. [61] were 11.08 and 10.96, respectively. This means that the PCM will exist uncharged within the pH range of 2.1 to 11.3 in the studied solution. As a result, electrostatic attraction is ruled out in this review, which is in line with previous research [62]. As a result, the adsorption capacities of PCM onto the prepared BC, and BC-H_3PO_4 are insignificantly different (Figs. 5 and S2). This characteristic is crucial from the standpoint of removal, since it eliminates the need for pH modifications when utilizing BM, BC, and BC-H_3PO_4 adsorbents to remove paracetamol. This result supports previous research that suggests the adsorption process is not electrostatic (pH_{pzc} in Table 1), as described in the literature for PCM with various adsorbents [50,63–65].

3.4. Isothermal models

From Table 2 and Fig. S3, it can be seen that the regression coefficient (R^2, χ^2, $F_{error\%}$, AIC and $AIC_{corrected}$) of the Langmuir and D-R equations (($R^2 > 0.9964$, $\chi^2 < 0.476$, $F_{error\%} < 1.81$, AIC < 3.148 and $AIC_{corrected} < 16.117$) is more fitted when compared with that of the Freundlich equation ($R^2 > 0.8384$, $\chi^2 < 5.239$, $F_{error\%} < 8.328$, AIC < 47.393 and $AIC_{corrected} < 52.193$) reveals that Langmuir and D-R isotherms is efficient in correlating the isotherm data. These results implying that the adsorption of BM, BC, and BC-H_3PO_4 models on heterogeneous surfaces involves a complicated mechanism comprising both monolayer and multilayer adsorption. The data in Table 2 indicate that the maximum adsorption capacities q_{max} estimated from Langmuir isotherm model at 25°C for paracetamol were 99.010, 166.667 and 256.10 mg/g onto BM, BC and BC-H_3PO_4, respectively. The Langmuir equation was further examined using a dimensionless constant known as the Langmuir separation factor (R_L) [Eq. (7)], which reflects the adsorption's favorability. The R_L values in this investigation were between 0 and 1 (0.037–0.128) (Table 2), showing that PCM adsorption onto BM, BC, and BC-H_3PO_4 was favorable. The n values calculated from the Freundlich isotherm model are greater than 1.00, suggesting that the adsorption of PCM onto adsorbents is favorable.

adsorption capacities q_{max} and the adsorption free energy (E_{DR}) are calculated using D-R isotherm model for the PCM removal from the aqueous phase by BM, BC and BC-H_3PO_4 and are listed in Table 2. The difference in q_{max} between the Langmuir and D-R models could be due to various definitions of q_{max} in the two models. The D-R represents the maximum PCM adsorption at the adsorbent's entire unique microspores volume, whereas q_{max} represents the maximum PCM adsorption at monolayer coverage in Langmuir. As a result, the value of q_{max} obtained from the Langmuir model is greater than the value obtained from the D-R model [65].

If E_{DR} is less than 8 (kJ/mol), chemical ion exchange if E_{DR} is between 8–16 (kJ/mol), and particle diffusion if E_{DR} is larger than 16 (kJ/mol), the adsorption is driven by physical forces [66,67]. The experimental E_{DR} values were found to range from 0.118 to 2.505 kJ/mol, demonstrating the physical adsorption of PCM onto BM, BC, and BC-H_3PO_4 surfaces.

The maximum adsorption capacity (q_{max} mg/g) is critical for determining which adsorbent has the best efficiency and is useful for scaling up considerations. For PCM adsorption, some studies use different activated carbon prepared from agriculture waste. Table 3 shows that BM, BC and BC-H_3PO_4 has a higher or comparable adsorption capacity to the adsorbents mentioned in the literature [50,62,64,68–71], indicating that it is suitable for removing PCM from aqueous solutions.

Table 2
Isotherm parameters for PCM adsorption on BM, BC and BC-H_3PO_4. Initial PCM concentration 10–100 mg/L; pH = 7.0; adsorbent dosage 0.15 g/50 mL; temperature 25°C

Isotherm model	Parameter	BM	BC	BC-H_3PO_4
Langmuir	q_{max} (mg/g)	99.010	166.667	256.410
	K_L (L/g)	0.119	0.259	0.068
	R_L	0.078	0.037	0.127
	R^2	0.9964	0.9995	0.9996
	χ^2	0.087	0.003	0.025
	$F_{error\%}$	1.45	0.24	0.49
	AIC	3.148	2.917	2.522
	$AIC_{corrected}$	7.948	16.117	5.052
Freundlich	K_F [(mg/g)(L/mg)$^{1/n}$]	2.864	8.410	6.034
	n	3.634	6.309	3.233
	R^2	0.8896	0.8412	0.9301
	χ^2	3.024	2.621	5.239
	$F_{error\%}$	8.38	5.59	7.25
	AIC	35.074	39.452	47.393
	$AIC_{corrected}$	39.874	44.252	52.193
D-R	q_{max} (mg/g)	87.243	156.413	209.474
	E (kJ/mol)	2.222	3.084	1.936
	R^2	0.9971	0.9982	0.9977
	χ^2	0.042	0.025	0.746
	$F_{error\%}$	1.81	0.58	1.56
	AIC	1.229	1.544	2.790
	$AIC_{corrected}$	6.029	3.255	3.703

3.5. Effect of contact time and adsorption kinetic

The effects of contact time on the PCM's adsorption capability are shown in Fig. 6. Due to the large number of unoccupied sites available on the surface of the adsorbent, the adsorption of PCM was quickly increased at the start of the process up to 30 min, as shown in Fig. 6. As the adsorption progressed, the PCM molecules occupied more active sites, increasing the resistance of PCM aggregation to diffuse deeper into the adsorbent and lowering the adsorption rate. As a result, the removal rate was gradually increased over time until it reached equilibrium after 120 min, suggesting that the adsorption sites on BM, BC and BC-H_3PO_4 had been saturated [72]. The adsorption performance demonstrated in this study is similar to that reported by Dutta et al. [73] and Mukoko et al. [74], who found that when tea waste and rice hull generated activated carbon were utilized, adsorption of PCM reached equilibrium in less than 60 min.

The experiment data were fitted to three generally used models to analyze the kinetic adsorption process: pseudo-first-order (Eq. 11), pseudo-second-order (Eq. 12), and intraparticle diffusion (Eq. 13) [62]. Fig. S4 shows the adsorption kinetic parameters for PCM removal, which are listed in Table 4. In comparison to the pseudo-first-order model ($R^2 > 0.6135$, $\chi^2 < 256.289$, $F_{error\%} < 235.61$, AIC < 108.745 and $AIC_{corrected} < 112.174$), the pseudo-second-order model had the highest correlation coefficient R^2 ($R^2 > 0.9987$) and provided the lowest χ^2, $F_{error\%}$, AIC and $AIC_{corrected}$ ($\chi^2 < 0.290$, $F_{error\%} < 1.09$, AIC < 16.079 and $AIC_{corrected} < 19.507$). As a result, the pseudo-second-order model is more suited to describe the adsorption kinetics. The fact that the q_e value derived using the pseudo-second-order is closer to the experimental q_e value supports this. This discovery is in line

Table 3
Comparison between the maximum monolayer adsorption capacity (q_{max}, mg/g) of PCM on various adsorbents

Adsorbent	Conditions		q_{max} (mg/g)	Reference
	pH	T/°C		
Grape stalk	6.0	20	2.18	[62]
Spent tea leave/H_3PO_4	7.0	25	59.2	[64]
Oak fruits/H_3PO_4	7.0	25	45.45	[50]
Pine wood/K_2CO_3	7.0	30	243.9	[68]
Peach stones	5.8	30	113.0	[69]
Pre-treated cork/KOH	7.0	30	118.6	[70]
Spherical pomelo peel wastes	7.0	25	286.0	[71]
Non-spherical pomelo peel wastes			147.0	
BM	7.0	25	19.46	This work
			41.21	
BC	7.0	25	47.67	This work
			55.48	
BC-H_3PO_4	7.0	25	34.96	This work

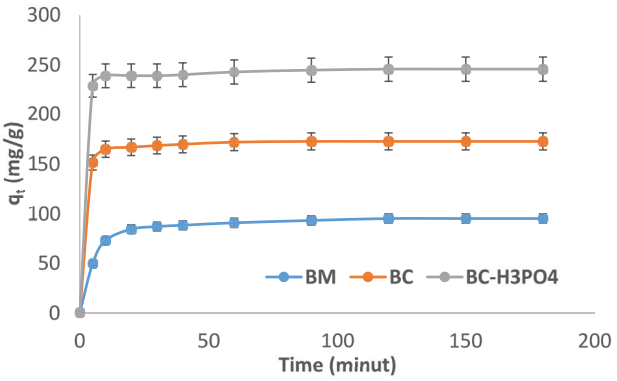

Fig. 6. Effect of contact time on the BM, BC and BC-H_3PO_4 adsorption efficiency for PCM. Initial PCM concentration 50 mg/L; pH = 7.0; adsorbent dosage 0.15 g/50 mL; temperature 25°C.

with the findings of a number of study groups, including Ferreira et al. [75,76].

The intra-particle diffusion kinetic model C values (80.145, 163.650, and 235.410 for BM, BC, and BC-H_3PO_4, respectively) did not cross from the original point ($C \neq 0$), as shown in Table 4. As a result, it can be stated that intra-particle diffusion was not the only rate-limiting step in the adsorbents removal of PCM.

3.6. Effect of temperature

The thermodynamics of PCM adsorption onto BM, BC and BC-H_3PO_4 were investigated using an calculated change in standard Gibbs free energy change ($\Delta G°$), enthalpy change ($\Delta H°$) and entropy change ($\Delta S°$). The thermodynamic parameters are calculated based on the laws of thermodynamics using the Van't Hoff equation as defined in the Eqs. (20)–(22) [77].

Table 4
Kinetic parameters for PCM adsorption onto BM, BC and BC-H_3PO_4. Initial PCM concentration 50 mg/L; pH = 7.0; adsorbent dosage 0.15 g/50 mL; temperature 25°C

System	BM	BC	BC-H_3PO_4
$q_{e,exp}$ (mg/g)	99.010	166.667	256.410
Pseudo-first-order			
$q_{e,cal}$ (mg/g)	89.586	159.050	223.632
k_1 (1/min)	0.033	0.036	0.027
R^2	0.7534	0.6685	0.6135
χ^2	25.625	121.226	256.289
$F_{error\%}$	99.46	182.36	235.61
AIC	77.101	96.930	108.745
$AIC_{corrected}$	80.438	100.359	112.174
Pseudo-second-order			
$q_{e,cal}$ (mg/g)	96.154	162.414	253.902
k_2 (g/mg min)	0.004	0.009	0.008
R^2	0.9988	0.9994	0.9987
χ^2	0.118	0.093	0.290
$F_{error\%}$	1.09	0.59	0.33
AIC	4.779	9.554	16.079
$AIC_{corrected}$	8.208	12.982	19.507
Intraparticle diffusion equation			
k_{id}	1.221	0.744	0.828
C	80.145	163.650	235.410
R^2	0.9989	0.9995	0.9999
χ^2	0.102	0.070	0.031
$F_{error\%}$	0.97	0.59	0.33
AIC	4.102	6.749	1.676
$AIC_{corrected}$	7.530	10.177	5.105

Table 5
Thermodynamic parameters for PCM adsorption on BM, BC and BC-H_3PO_4

Adsorbent	T/K	Van't Hoff equation	$\ln K_d$	$-\Delta G°$ (kJ/mol)	$-\Delta H°$ (kJ/mol)	$-\Delta S°$ (J/K mol)
PCM/BM	298.15	$y = 5{,}642.4x + 11.925$ $R^2 = 0.9854$	6.906	17.119	46.911	99.144
	308.15		6.581	16.861		
	318.15		5.710	15.104		
PCM/BC	298.15	$y = 12{,}861.0x + 37.308$ $R^2 = 0.9980$	5.884	14.585	106.926	310.112
	308.15		4.315	11.055		
	318.15		3.176	8.401		
PCM/ BC-H_3PO_4	298.15	$y = 11{,}798.0x + 33.190$ $R^2 = 0.9974$	6.346	15.731	98.89	275.942
	308.15		5.171	13.249		
	318.15		3.856	10.200		

$$\Delta G° = -RT \ln K_d \tag{20}$$

$$\Delta G° = \Delta H° - T\Delta S° \tag{21}$$

$$\ln K_d = -\frac{\Delta H°}{RT} + \frac{\Delta S°}{R} \tag{22}$$

The equilibrium constant K_d is estimated at each temperature as a dimensionless parameter by multiplying the Langmuir constant (K_L) by the atomic mass of PCM (151 g/mol), and then by 55.55 (the number of moles of pure water per liter) [78], where R (8.314 J/mol K) is the gas constant, T (K) is the absolute temperature, and T (K) is the absolute temperature. The values $\Delta S°$ and $\Delta H°$ can be determined from the slopes and intercepts of a graph of $\ln K_c$ vs. $1/T$.

Since the Gibbs free energy ($\Delta G°$) for the entire studied solution temperature range is negative, the measurement results (Table 5) indicated that the adsorption process occurred spontaneously. Furthermore, the exothermic nature of PCM adsorption onto the BM, BC, and BC-H_3PO_4 is shown by the negative value of the enthalpy transition ($\Delta H°$). This corresponds to the K_d constant in Table 5; the equilibrium constant's value decrease as the temperature increase. The adsorption of PCM onto porous carbonaceous materials, according to some studies [63,64], is an exothermic process ($\Delta H°$). Furthermore, the entropy change ($\Delta S°$) is negative, meaning that during the adsorption process, PCM organization at the adsorbents/solution interface gets more ordered.

4. Conclusions

BC-H_3PO_4 from PFS wastes was successfully produced via chemical activation with H_3PO_4 and was subsequently used to remove PCM from aqueous solution in this investigation. As indicated by nitrogen adsorption–desorption analyses and SEM micrographs, H_3PO_4 treatment resulted in the creation of high surface area and pore volume in BC-H_3PO_4. Within 60 min, the process for removing PCM from solution using BM, BC, and BC-H_3PO_4 had reached a rapid equilibrium state. BM, BC, and BC-H_3PO_4 had maximum Langmuir adsorption capacities of 99.010, 166.667, and 256.10 mg/g toward PCM, respectively. Adsorption kinetics analysis revealed that the data is well-fitted to the pseudo-second-order model. The analysis result revealed the influence of intraparticle diffusion, however it was not the rate-limiting phase, and the adsorption process involves more than one phase. The adsorption of PCM molecules at the solid/liquid interface proceeded spontaneously ($\Delta G° < 0$) and was exothermic in nature ($\Delta H° < 0$), with the organization of PCM molecules at the interface becoming more orderly during the adsorption process ($\Delta S° < 0$).

Acknowledgment

The authors acknowledge The University of Jordan for supporting this research.

References

[1] L. Wang, Z. Bian, Photocatalytic degradation of paracetamol on Pd-$BiVO_4$ under visible light irradiation, Chemosphere, 239 (2020) 124815, doi: 10.1016/j.chemosphere.2019.124815.
[2] C. Akay, U. Tezel, Biotransformation of Acetaminophen by intact cells and crude enzymes of bacteria: a comparative study and modelling, Sci. Total Environ., 703 (2019) 134990, doi: 10.1016/j.scitotenv.2019.134990.
[3] I. Bavasso, C. Poggi, E. Petrucci, Enhanced degradation of paracetamol by combining UV with electrogenerated hydrogen peroxide and ozone, J. Water Process Eng., 34 (2020) 101102, doi: 10.1016/j.jwpe.2019.101102.
[4] Q. Zhang, S. Cheng, H. Xia, L. Zhang, J. Zhou, C. Li, J. Shu, X. Jiang, Paracetamol degradation performance and mechanisms using microwave-assisted heat-activated persulfate in solutions, Water Air Soil Pollut., 230 (2019) 271, doi: 10.1007/s11270-019-4286-7.
[5] R. Katal, M.H.D.A. Farahani, H. Jiangyong, Degradation of acetaminophen in a photocatalytic (batch and continuous system) and photoelectrocatalytic process by application of faceted-TiO_2, Sep. Purif. Technol., 230 (2020) 115859, doi: 10.1016/j.seppur.2019.115859.
[6] M. Gros, S. Rodríguez-Mozaz, D. Barceló, Fast and comprehensive multiresidue analysis of a broad range of human and veterinary pharmaceuticals and some of their metabolites in surface and treated waters by ultra-high-performance liquid chromatography coupled to quadrupole-linear ion trap tandem mass spectrometry, J. Chromatogr., A, 1248 (2012) 104–121.
[7] F.C. Wu, R.L. Tseng, R.S. Juang, Initial behavior of intraparticle diffusion model used in the description of adsorption kinetics, Chem. Eng. J., 153 (2009) 1–8.
[8] S. Fekadu, E. Alemayehu, R. Dewil, B. Van der Bruggen, Pharmaceuticals in freshwater aquatic environments: a comparison of the African and European challenge, Sci. Total Environ., 654 (2019) 324–337.

[9] M. Neamțu, M. Bobu, A. Kettrup, I. Siminiceanu, Ozone photolysis of paracetamol in aqueous solution, J. Environ. Sci. Health. Part A Toxic/Hazard. Subst. Environ. Eng., 48 (2013) 1264–1271.
[10] R. Andreozzi, V. Caprio, R. Marotta, D. Vogna, Paracetamol oxidation from aqueous solutions by means of ozonation and H_2O_2/UV system, Water Res., 37 (2003) 993–1004.
[11] A.Z. Yavas, Y. Mizukoshi, Y. Maeda, N.H. Ince, Supporting of pristine TiO_2 with noble metals to enhance the oxidation and mineralization of paracetamol by sonolysis and sonophotolysis, Appl. Catal., B, 172–173 (2015) 7–17.
[12] M.D. De Luna, M.L. Veciana, C.C. Su, M.C. Lu, Acetaminophen degradation by electro-Fenton and photoelectro-Fenton using a double cathode electrochemical cell, J. Hazard. Mater., 30 (2012) 217–218.
[13] S. Basha, D. Keane, K. Nolan, M. Oelgemöller, J. Lawler, J.M. Tobin, A. Morrissey, UV-induced photocatalytic degradation of aqueous acetaminophen: the role of adsorption and reaction kinetics, Environ. Sci. Pollut. Res., 22 (2015) 2219–2230.
[14] M.A.L. Zavala, C.R.J. Lara, Degradation of paracetamol and its oxidation products in surface water by electrochemical oxidation, Environ. Eng. Sci., 35 (2018) 1248–1254.
[15] R. Karaman, M. Khamis, J. Abbadi, A. Amro, M. Qurie, I. Ayyad, F. Ayyash, O. Hamarsheh, R. Yaqmour, S. Nir, S.A. Bufo, L. Scrano, S. Lerman, S. Gur-Reznik, C.G. Dosoretz, Paracetamol biodegradation by activated sludge and photocatalysis and its removal by a micelle-clay complex, activated charcoal and reverse osmosis membranes, Environ. Technol., 37 (2016) 2414–2427.
[16] M.A. Khana, B.H. Hameed, J. Lawler, M. Kumar, B.H. Jeond, Developments in activated functionalized carbons and their applications in water decontamination: a review, Desal. Water Treat., 54 (2015) 422–449.
[17] M. Ghaedi, A. Ansari, M.H. Habibi, A.R. Asghari, Removal of malachite green from aqueous solution by zinc oxide nanoparticle loaded on activated carbon: kinetics and isotherm study, J. Ind. Eng. Chem., 20 (2013) 17–28.
[18] T. Xie, K.R. Reddy, C. Wang, E. Yargicoglu, K. Spokas, Characteristics and applications of biochar for environmental remediation: a review, Crit. Rev. Env. Sci. Technol., 45 (2015) 939–969.
[19] J.D. Toth, Z. Dou, Use and Impact of Biochar and Charcoal in Animal Production Systems, M. Guo, Z. He, S.M. Uchimiya, Eds., Agricultural and Environmental Applications of Biochar: Advances and Barriers, ASPEC Publication, Madison, USA, 2016, pp. 199–224.
[20] M.J. Prauchne, F.R. Reinoso, Chemical versus physical activation of coconut shell: a comparative study, Microporous Mesoporous Mater., 152 (2012) 163–171.
[21] A.M. Aldawsari, M.A. Khan, B.H. Hameed, Z.A. AlOthman, M.R. Siddiqui, A. Yacine Badjah-Hadj-Ahmed, I.H. Alsohaimi, Development of activated carbon from *Phoenix dactylifera* fruit pits: process optimization, characterization, and methylene blue adsorption, Desal. Water Treat., 62 (2017) 273–281.
[22] M. Yusuf, F.M. Elfghi, S.A. Zaidi, E.C. Abdullaha, M.A. Khan, Applications of graphene and its derivatives as an adsorbent for heavy metal and dye removal: a systematic and comprehensive overview, RSC Adv., 5 (2015) 50392–50420.
[23] A.S. Mestre, A.S. Bexiga, M. Proença, M. Andrade, M.L. Pinto, I.I.M. Matos, I. Fonseca, A.P. Carvalho, Activated carbons from sisal waste by chemical activation with K_2CO3: kinetics of paracetamol and ibuprofen removal from aqueous solutions, Bioresour. Technol., 102 (2011) 8253–8260.
[24] A. Kumar, H.M. Jena, Preparation and characterization of high surface area activated carbon from Fox nut (*Euryale ferox*) shell by chemical activation with H_3PO_4, Results Phys., 6 (2016) 651–658.
[25] G.O. El-Sayed, M.M. Yehia, A.A. Asaad, Assessment of activated carbon prepared from corncob by chemical activation with phosphoric acid, Water Resour. Ind., 7–8 (2014) 66–75.
[26] A.I. Almendros, M.A. Martin-Lara, A. Ronda, A. Perez, G. Blazquez, M. Calero, Physico-chemical characterization of pine cone shell and its use as biosorbent and fuel, Bioresour. Technol., 196 (2015) 406–412.
[27] M.A. Lara, G. Blazquez, A. Ronda, M. Calero, Kinetic study of the pyrolysis of pine cone shell through non-isothermal thermogravimetry: effect of heavy metals incorporated by biosorption, Renewable Energy, 96 (2016) 613–624.
[28] N.M. Mahmoodi, B. Hayati, M. Arami, C. Lan, Adsorption of textile dyes on pine cone from colored wastewater: kinetic, equilibrium and thermodynamic studies, Desalination, 268 (2011) 117–125.
[29] G. Vazquez, J.G. Alvarez, A.I. Garcıa, M.S. Freire, G. Antorrena, Adsorption of phenol on formaldehyde-pretreated *Pinus pinaster* bark: equilibrium and kinetics, Bioresour. Technol., 98 (2007) 1535–1540.
[30] T. Calvete, E.C. Lima, N.F. Cardoso, J.C.P. Vaghetti, S.L.P. Dias, F.A. Pavan, Application of carbon adsorbents prepared from Brazilian-pine fruit shell for the removal of reactive orange 16 from aqueous solution: kinetic, equilibrium, and thermodynamic studies, J. Environ. Manage., 91 (2007) 1695–1706.
[31] D. Fatih, Dye biosorption from water employing chemically modified calabrian pine cone shell as an effective biosorbent, Environ. Prog. Sustainable Energy, 34 (2015) 1267–1278.
[32] M. Momoilovic, M. Purenovic, A. Bojic, A. Zarubica, M. Ranđelovic, Removal of lead(II) ions from aqueous solutions by adsorption onto pine cone activated carbon, Desalination, 276 (2011) 53–59.
[33] G. Duman, Y. Onal, C. Okutucu, S. Onenc, J. Yanik, Production of activated carbon from pine cone and evaluation of its physical, chemical, and adsorption properties, Energy Fuels, 23 (2009) 2197–2204.
[34] N. Mohammed, R. Abu-Zurayk, I. Hamadneh, A. Al-Dujaili, Phenol adsorption on biochar prepared from the pine fruit shells: equilibrium, kinetic and thermodynamics studies, J. Environ. Manage., 226 (2018) 377–385.
[35] F. Boudrahem, I. Yahiaoui, S. Saidi, K. Yahiaoui, L. Kaabache, M. Zennache, F.A. Benissad, Adsorption of pharmaceutical residues on adsorbents prepared from olive stones using mixture design of experiments model, Water Sci. Technol., 80 (2019) 1–12.
[36] I.D. Mall, V.C. Srivastava, G.V.A. Kumar, I.M. Mishra, Characterization and utilization of mesoporous fertilizer plant waste carbon for adsorptive removal of dyes from aqueous solution, Colloids Surf., A, 278 (2006) 175–187.
[37] F.A. Adekola, H.I. Adegoke, Adsorption of blue-dye on activated carbons produced from rice husk, coconut shell and coconut coirpith, Ife J. Sci., 7 (2005) 151–157.
[38] ASTM Standard Standard Test Method for Total Ash Content of Activated Carbon, Designation, 518 (2000) D2866–D2894.
[39] I. Langmuir, The adsorption of gases on plane surface of glass, mica and platinum, J. Am. Chem. Soc., 40 (1918) 1361–1403.
[40] H.M.F. Freundlich, About the adsorption, Zeitschrift für Physikalische Chemie, 57 (1906) 385–470.
[41] M.M. Dubinin, E.D. Zaverina, L.V. Radushkevich, Sorption and structure of active carbon I. Adsorption of organic vapors, J. Phys. Chem. A, 21 (1947) 1351–1362.
[42] D. Datta, H. Uslu, S. Kumar, Adsorptive separation of Cu^{2+} from an aqueous solution using trioctylamine supported montmorillonite, J. Chem. Eng. Data, 60 (2015) 3193–3200.
[43] S. Lagergren, About the theory of so-called adsorption of soluble substances, Kungliga Svenska Vetenskapsakademiens Handlingar, 24 (1898) 1–39.
[44] Y.S. Ho, Review of second-order models for adsorption systems, J. Hazard. Mater., 36 (2006) 681–689.
[45] S. Wu, L. Zhang, J. Chen, Paracetamol in the environment and its degradation by microorganisms, Appl. Microbiol. Biotechnol., 96 (2012) 875–884.
[46] A. El Hanandeha, Z. Mahdi, M.S. Imtiaz, Modelling of the adsorption of Pb, Cu and Ni ions from single and multi-component aqueous solutions by date seed derived biochar: comparison of six machine learning approaches, Environ. Res., 192 (2021) 110338, doi: 10.1016/j.envres.2020.110338.
[47] M.C. Silva, L. Spessato, T.L. Silva, G.K.P. Lopes, H.G. Zanella, J.T.C. Yokoyama, A.L. Cazetta, V.C. Almeida, H_3PO_4–activated carbon fibers of high surface area from banana tree pseudo-stem fibers: adsorption studies of methylene blue dye in

batch and fixed bed systems, J. Mol. Liq., 324 (2020) 114771, doi: 10.1016/j.molliq.2020.114771.
[48] G.K. Rajahmundry, C. Garlapati, P.S. Kumar, R.S. Alwi, D.V.N. Vo, Statistical analysis of adsorption isotherm models and its appropriate selection, Chemosphere, 276 (2021) 130176, doi: 10.1016/j.chemosphere.2021.130176.
[49] M.S. Shamsuddin, N.R.N. Yusoff, M.A. Sulaiman, Synthesis and characterization of activated carbon produced from Kenaf core fiber using H_3PO_4 activation, Procedia Chem., 19 (2016) 558–565.
[50] H. Nourmoradi, K.F. Moghadam, A. Jafari, B. Kamarehie, Removal of acetaminophen and ibuprofen from aqueous solutions by activated carbon derived from *Quercus Brantii* (Oak) acorn as a low-cost biosorbent, J. Environ. Chem. Eng., 6 (2018) 6807–6815.
[51] S. Wong, N.A.N. Yaccob, N. Ngadi, O. Hassan, I.M. Inuwa, From pollutant to solution of wastewater pollution: synthesis of activated carbon from textile sludge for dyes adsorption, Chin. J. Chem. Eng., 26 (2018) 870–878.
[52] B. Cantrell, G. Hunt, M. Uchimiya, M. Novak, S. Ro, Impact of pyrolysis temperature and manure source on physico-chemical characteristics of biochar, Bioresour. Technol., 107 (2012) 419–428.
[53] P. Fu, W. Yi, X. Bai, Z. Li, S. Hu, J. Xiang, Effect of temperature on gas composition and char structural features of pyrolyzed agricultural residues, Bioresour. Technol., 102 (2011) 8211–8219.
[54] Y. Chen, G. Dai, Q. Gao, Starch nanoparticles−graphene aerogels with high supercapacitor performance and efficient adsorption, ACS Sustainable Chem. Eng., 7 (2019) 14064−14073.
[55] D.C.J. Valle, M.G. Corzo, J.P. Villegas, V.G. Serrano, Study of cherry stones as BM in preparation of carbonaceous adsorbents, J. Anal. Appl. Pyrolysis, 73 (2005) 59–67.
[56] L. Pei, J. Zhou, L. Zhang, Preparation and properties of Ag-coated activated carbon nanocomposites for indoor air quality control, Build. Environ., 63 (2013) 108–113.
[57] A. Puziy, O. Poddubnay, M. Alonso, A.S. Garcıa, F.J. Tascón, Synthetic carbons activated with phosphoric acid: I. Surface chemistry and ion binding properties, Carbon, 40 (2002) 1493–1505.
[58] A. Kumar, H.M. Jena, Preparation and characterization of high surface area activated carbon from Fox nut (*Euryale ferox*) shell by chemical activation with H_3PO_4, Results Phys., 6 (2016) 651–658.
[59] S.M. Yakout, Physico-chemical characteristics of biochar produced from rice straw at different pyrolysis temperature for soil amendment and removal of organics, Proc. Natl. Acad. Sci. India: Sect. A: Phys. Sci., 87 (2017) 207–214.
[60] O. Tepe, Z. Tunç, B. Yıldız, M. Şahin, Efficient removal of paracetamol by manganese oxide octahedral molecular sieves (OMS-2) and persulfate, Water Air Soil Pollut., 238 (2020) 231–246.
[61] M.A. Elbagerma, G. Azimi, H.G.M. Edwards, A.I. Alajtal, I.J. Scowen, *In-situ* monitoring of pH titration by Raman spectroscopy, Spectrochim. Acta, Part A, 75 (2010) 1403–1410.
[62] I. Villaescusa, N. Fiol, J. Poch, A. Bianchi, C. Bazzicalupi, Mechanism of paracetamol removal by vegetable wastes: the contribution of π–π interactions, hydrogen bonding and hydrophobic effect, Desalination, 270 (2011) 135–142.
[63] M.A. Khan, Z.A. AlOthman, M. Kumar, M.S. Ola, M.R. Siddique, Biosorption potential assessment of modified pistachio shell waste for methylene blue: thermodynamics and kinetics study, Desal. Water Treat., 56 (2015) 146–160.
[64] S. Wong, Y. Lim, N. Ngadi, R. Mat, O. Hassan, I. Inuwa, N.B. Mohamed, J.H. Low, Removal of acetaminophen by activated carbon synthesized from spent tea leaves: equilibrium, kinetics and thermodynamics studies, Powder Technol., 338 (2018) 878–886.
[65] A.M. Salehi, G. Moussavi, Removal of acetaminophen from the contaminated water using adsorption onto carbon activated with NH_4Cl, Desal. Water Treat., 57 (2016) 12861–12873.
[66] S.I.Y. Salameh, F.I. Khalili, A.H. Al-Dujaili, Removal of U(VI) and Th(IV) from aqueous solutions by organically modified diatomaceous earth: evaluation of equilibrium, kinetic and thermodynamic data, Int. J. Miner. Process., 168 (2017) 9–18.
[67] M. Ghaedi, A.M. Ghaedi, E. Negintaji, A. Ansari, A. Vafaei, M. Rajabi, Random forest model for removal of bromophenol blue using activated carbon obtained from *Astragalus bisulcatus* tree, J. Ind. Eng. Chem., 20 (2014) 1793–1803.
[68] M. Galhetas, A.S. Mestre, M.L. Pinto, I. Gulyurtlu, H. Lopes, A.P. Carvalho, Carbon-based materials prepared from pine gasification residues for acetaminophen adsorption, Chem. Eng. J., 240 (2014) 344–351.
[69] I. Cabrita, B. Ruiz, A.S. Mestre, I.M. Fonseca, I.P. Carvalho, C.O. Ania, Removal of an analgesic using activated carbons prepared from urban and industrial residues, Chem. Eng. J., 63 (2010) 249–255.
[70] A.S. Mestre, R.A. Pires, I. Aroso, E.M. Fernandes, M.L. Pinto, R.L. Reis, M.A. Andrade, J. Pires, S.P. Silva, A.P. Carvalho, Activated carbons prepared from industrial pre-treated cork: sustainable adsorbents for pharmaceutical compounds removal, Chem. Eng. J., 253 (2014) 408–417.
[71] H.N. Tran, F. Tomul, H.T.H. Nguyen, D.T. Nguyen, E.C. Lima, G.T. Le, C.T. Chang, V. Masindi, S.H. Woo, Innovative spherical biochar for pharmaceutical removal from water: insight into adsorption mechanism, J. Hazard. Mater., 349 (2020) 122255, doi: 10.2136/sssaspecpub63.2014.0043.5.
[72] S. Rangabhashiyam, N. Anu, M.S.G. Nandagopal, N. Selvaraju, Relevance of isotherm models in biosorption of pollutants by agricultural by-products, J. Environ. Chem. Eng., 2 (2014) 398–414.
[73] M. Dutta, U. Das, S. Mondal, S. Bhattachriya, R. Khatun, R. Bagal, Adsoption of acetaminophen by using tea waste derived activated carbon, Int. J. Environ. Sci., 6 (2015) 270–280.
[74] T. Mukoko, M. Mupa, U. Guyo, F. Dziike, Preparation of rice hull activated carbon for the removal of selected pharmaceutical waste compound in hospital effluent, Environ. Anal. Toxicol., S7 (2015) 008, doi: 10.4172/2161-0525.S7-008.
[75] R.C. Ferreira, H.H.C.D. Lima, A.A. Candido, O.M.C. Junior, P.A. Arroyo, K.Q.D. Carvalho, G.F. Gauze, M.A.S.D. Barros, Adsorption of paracetamol using activated carbon of dende and babassu coconut mesocarp, Int. J. Biomol. Agric. Food Biotechnol. Eng., 9 (2015) 575–580.
[76] M. Ghaedi, A. Ansari, R. Sahraei, ZnS:Cu nanoparticles loaded on activated carbon as novel adsorbent for kinetic, thermodynamic and isotherm studies of Reactive orange 12 and Direct yellow 12 adsorption, Spectrochim. Acta, Part A, 114 (2013) 687–694.
[77] I. Hamadneh, N.W. Al-Jundub, A.A. Al-Bshaish, A.H. Al-Dujiali, Adsorption of lanthanum(III), samarium(III), europium(III) and gadolinium(III) on raw and modified diatomaceous earth: equilibrium, kinetic and thermodynamic study, Desal. Water Treat., 215 (2021) 119–135.
[78] X. Zhou, X. Zhou, The unit problem in the thermodynamic calculation of adsorption using the Langmuir equation, Chem. Eng. Commun., 201 (2014) 1459–1467.

Supplementary information

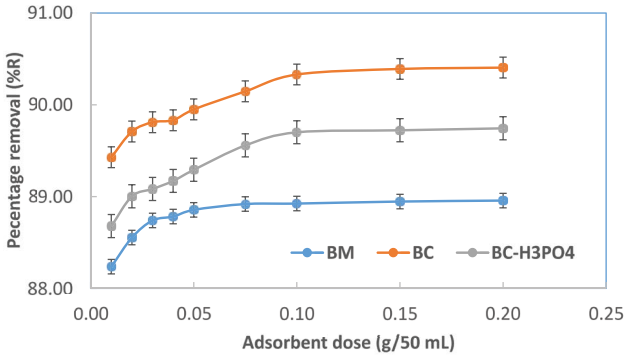

Fig. S1. Effect of BM, BC and BC-H_3PO_4 dosages. Initial PCM concentration 50 mg/L; pH = 7.0; temperature 25°C.

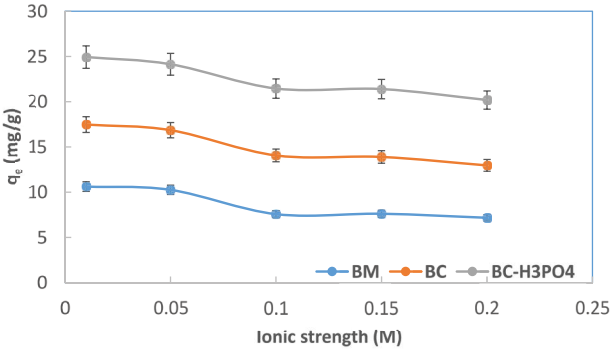

Fig. S2. Effect of ionic strength on the adsorption of Sm(III) and Nd(III) ions onto BM, BC and BC-H_3PO_4. Initial PCM concentration 50 mg/L; pH = 7.0; adsorbent dosage 0.15 g/50 mL; temperature 25°C.

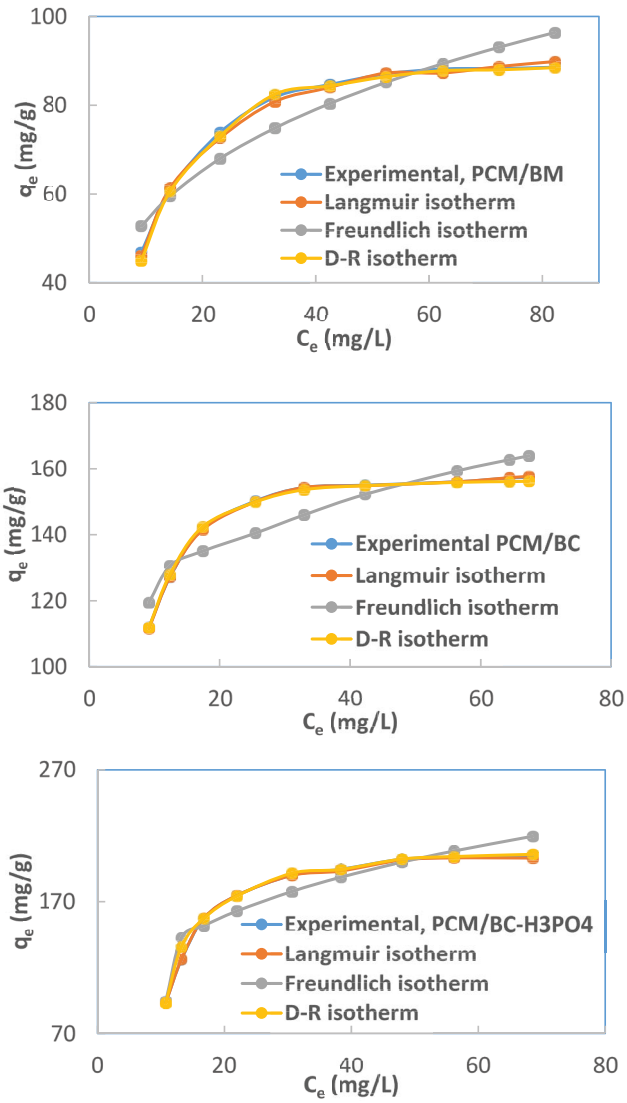

Fig. S3. Equilibrium isotherm for PCM adsorption on BM, BC and BC-H_3PO_4 adsorbents, using nonlinear regression method. Initial PCM concentration 10–100 mg/L; pH = 7.0; adsorbent dosage 0.15 g/50 mL; temperature 25°C.

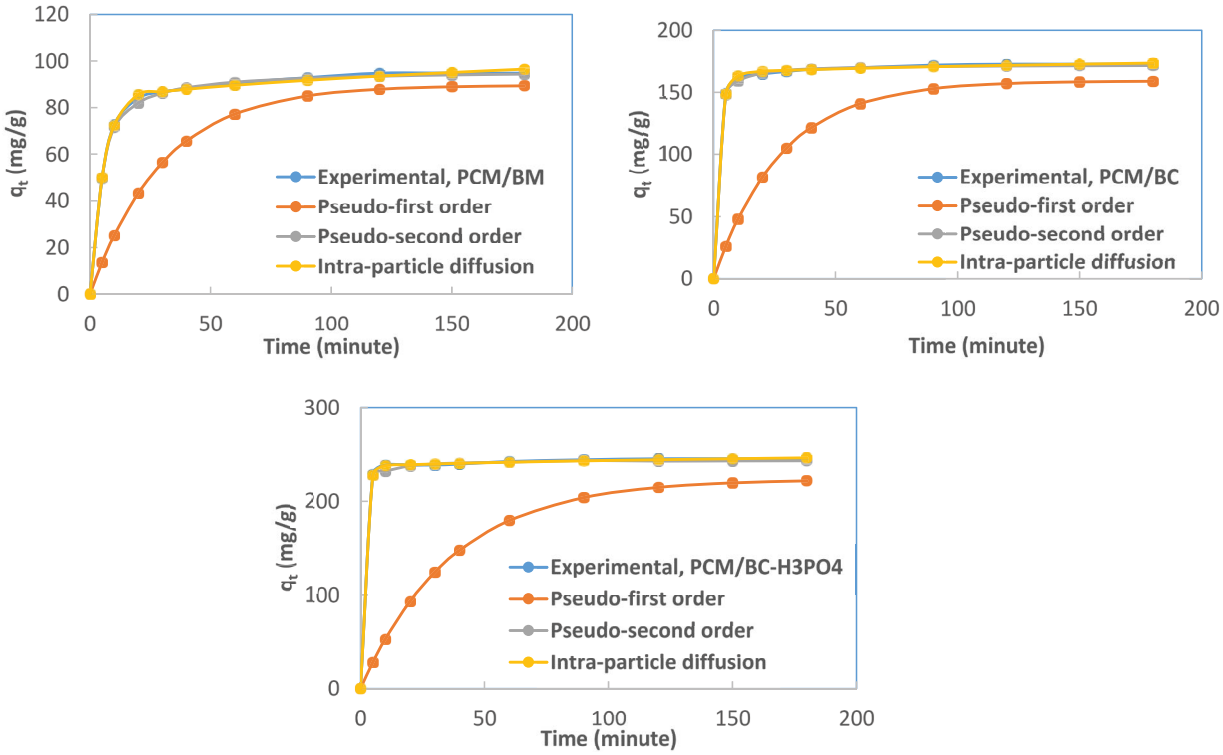

Fig. S4. Kinetic models for PCM adsorption on BM, BC and BC-H_3PO_4 adsorbents, using nonlinear regression method. Initial PCM concentration 50 mg/L; pH = 7.0; adsorbent dosage 0.15 g/50 mL; temperature 25°C.